lubricants

MDPI

Article

Experimental Investigations on Wear in Oscillating Grease-Lubricated Rolling Element Bearings of Different Size and Type

Gernot Bayer [1,*], Arne Bartschat [2], Sebastian Wandel [1], Sebastian Baust [3] and Gerhard Poll [1]

[1] Institute of Machine Design and Tribology (IMKT), Leibniz University Hannover, An der Universität 1, 30823 Garbsen, Germany; wandel@imkt.uni-hannover.de (S.W.)
[2] Fraunhofer Institute for Wind Energy Systems IWES, Am Schleusengraben 22, 21029 Hamburg, Germany; arne.bartschat@iwes.fraunhofer.de
[3] P. E. Concepts GmbH, Wiener Straße 5, 28359 Bremen, Germany
* Correspondence: bayer@imkt.uni-hannover.de

Abstract: Grease-lubricated rolling element bearings can suffer from wear due to lubricant starvation under certain oscillating operating conditions. Especially for large-scale slewing bearings, such as blade bearings in wind turbines, experimental investigations are complex compared to small-scale reference testing. For an easier manner of testing, it is desirable to know whether the results of small-scale testing are applicable to larger-sized bearings. In this work, three different bearing types were tested and compared to already published results from a small-scale ACBB with a pitch diameter of 60 mm. The newly tested bearing types comprise a downscaled blade bearing (4-point contact double row ball bearing) with a pitch diameter of 673 mm, a small-scale CRTB with a pitch diameter of 77.5 mm and another ACBB with a pitch diameter of 95 mm. Qualitatively, all tested bearings show similar wear behaviour in terms of friction energy when operation parameters are varied. With higher oscillation frequency, damage becomes more severe. The oscillation amplitude shows three distinctive regimes. Within the range of small amplitudes, an increase in amplitude leads to more pronounced damage. We observe a threshold amplitude where this is no longer the case; a further increase in amplitude counteracts wear initiation until a final threshold is reached, beyond which no more wear is observed. These findings are in accordance with the reference results of the small-scale ACBB. Direct comparison between point and line contact shows that the latter is more prone to wear initiation under grease-lubricated, oscillating operating conditions. Furthermore, a previously introduced empirical number shows good performance in assessing critical operating parameters of the different bearing types. Specifically, harmful operating conditions can be classified for all studied bearing types with an accuracy of 78%. This method can be useful to assess operating conditions of greased, oscillating, rolling element bearings, e.g., to assess different pitch controllers or designs of slewing bearings.

Keywords: blade bearing; false brinelling; grease lubrication; oscillating bearing; pitch bearing

Citation: Bayer, G.; Bartschat, A.; Wandel, S.; Baust, S.; Poll, G. Experimental Investigations on Wear in Oscillating Grease-Lubricated Rolling Element Bearings of Different Size and Type. *Lubricants* **2023**, *11*, 120. https://doi.org/10.3390/lubricants11030120

Received: 22 January 2023
Revised: 23 February 2023
Accepted: 2 March 2023
Published: 8 March 2023

1. Introduction

Highly loaded, oscillating, grease-lubricated rolling element bearings play a role in several technical applications. In comparison to oil lubrication, the analysis of grease lubrication can require specialised treatment [1]. Furthermore, the wear and fatigue behaviour of these bearings is mostly discussed in the context of blade bearings in wind turbines especially for those operated with an individual pitch controller (IPC) [2–5]. Load-mitigating controller design leads to a highly increased pitch activity [6]. Thus, the question arises whether frequent pitching can lead to critical damage in these bearings as is the case in small-scale laboratory testing or field failures such as false brinelling. Damage marks in oscillating bearings are physically distinguished by the ratio of the travelled distance by the

rolling element on the raceway between the upper and lower dead centre of the oscillation x to the width of the contact $2b$ parallel to the direction of rolling. If the ratio $\frac{x}{2b} < 1$, there are points on the raceway that are constantly part of the mechanical contact as long as the centre of the oscillation does not change. Under these conditions, a sticking zone usually emerges in the middle of the contact in which no relative motion between the contacting surfaces occurs. Therefore, the damage marks caused by these conditions show a distinctive central zone that is exempted from any wear due to the locally lacking relative motion that leads to adhesive or abrasive surface damage. In the following, these marks are called standstill marks since the described contact conditions often occur due to vibrations during the standstill of the bearing [7]. Nevertheless, there is no consensus on the naming in the literature [8–11].

On the other hand, operating conditions with $\frac{x}{2b} \geq 1$ provoke wear marks of a more uniform appearance. Mostly, they are referred to as false brinelling since the damage marks in an advanced stadium can be mistaken for indentation due to plastic deformation similar to the Brinell hardness test [7]. The investigations in this paper focus solely on the mechanism of false brinelling, i.e., fully open contacts. In comparison to standstill marks, there is less literature on the influence of the main oscillation parameters, namely the frequency f and the double amplitude of the inner ring φ (in the case of a locked outer ring). Phaner-Goutorbe et al. [12] tested grease-lubricated TBB with frequencies from 3 to 20 Hz and double amplitudes between 3° and 12°. They reported that, in this range, there was no significant difference in wear progress for the different parameter combinations of f and φ. There is no further comment on how this was judged. Although their STM-scans provide interesting insight into the process of damage development, information regarding friction torque and lubrication mechanisms are not directly provided. Maruyama et al. [13] used a similar test setup to investigate the mechanisms behind oil and grease lubrication under $\frac{x}{2b}$-ratios from 0.6 to 2. For $\frac{x}{2b} = 1.9$, they observe that the influence of the maximum rolling speed (2 to 100 $\frac{\text{mm}}{\text{s}}$) on the extent of the wear varies with the kinematic viscosity of the base oil. They judged the extent with an indicator formed by taking the ratio of the final surface roughness to the initial surface roughness. For thick base oils ($\nu = 396\ \frac{\text{mm}^2}{\text{s}}$), this indicator increased with higher speeds. Greases with thinner base oils ($\nu = 19\ \frac{\text{mm}^2}{\text{s}}$) showed the opposite behaviour for increasing maximum rolling velocities during an oscillation period. It is not fully clear whether conclusions regarding the wear measured by the change in surface roughness are compatible with other means of measuring wear such as weight loss or increase in friction torque. Moreover, the range of values of the $\frac{x}{2b}$-ratio from 0.6 to 2 covered by their experiments is relatively small and close to standstill marks, which are not the focus of this publication. Becker [14] showed that there is a strong correlation between an increase in friction torque and the indentation depth of damage marks. He compared the performance of different greases with and without additional contamination of salt water. Experimental investigations on the influence of the oscillation parameters were not mentioned. Cavacece et al. [15] investigated the oscillating endurance of a spherical roller bearing under a frequency of 5 Hz and an oscillation double amplitude of 40°. There is no comment on the kind of grease they used in their investigations with a maximum contact pressure of 4 GPa. They characterised damage evolution using the variation of the progression of the resistant torque over the course of an experiment and SEM scans. After smoothing during a run-in phase, the surfaces of a roller and raceway start to show detachments of the surface and plastic deformations. Continuing the experiment leads to deep pittings on the raceway surface. They compared their results to previous work of theirs dealing with DGBB [16]. Generally, they were able to identify the same phases in the resulting friction torque and similar changes on the raceway surfaces for both bearing types. The influence of frequency and double amplitude of the oscillating motion on the wear initiation was not addressed. Some publications with $\frac{x}{2b} \geq 1$ focus on the effect of grease composition and build-up of tribolayers [17–20]. Since this paper is focused more on the influence of oscillating operating conditions, e.g., induced by pitch controllers, these results dealing with tribolayer buildup and grease properties are not further discussed. In

the literature presented so far, the phenomenological course of the damage is already well documented. Comprehensive studies on the influence of the oscillation parameters on the initiation of the damage are not to be found, especially for higher $\frac{x}{2b}$ ratios. These points are of particular interest for the evaluation of pitch controllers or slewing bearing concepts for wind turbines.

A first systematic evaluation of the effect of the oscillation parameters on the friction torque was conducted by Wandel et al. [21]. They investigated oscillating ACBB of the designation 7208 acc. to [22,23] (pitch diameter 60 mm) with two different greases under double amplitudes from 2 to 45° and frequencies from 0.2 to 5 Hz. The tests were evaluated in terms of the friction torque and showed a clear result regarding the influence of the oscillation parameters. Higher frequencies lead to a more severe damage, mostly independent of the actual double amplitude. The amplitude influence is threefold: up to a certain amplitude, the damage increases with higher angles. Beyond this threshold, further increase in amplitude reduces bearing damage. After reaching a second threshold, no more wear is observed. Wandel et al. assume that the root cause for wear under greased oscillating conditions is a mechanism similar to starvation for rolling conditions, i.e., a lack of lubricant around the contact area [24]. The base oil on the rolling track that was released by the thickener structure is displaced by the rolling elements due to their oscillating motion and partly removed from the path of the contact. A counteracting flow driven by capillary forces around the rolling element brings new oil into the contact. If the displacement flow outweighs the replenishing flow, the initial amount of base oil around the contact will diminish with an increasing cycle number. When a critical amount of remaining base oil is undershot, the remaining base oil is not able to prevent adhesive wear between the rolling partners in the presumably prevailing boundary or mixed lubrication regime. Based on their experimental observations and the described concept, Wandel et al. propose the following empirical, dimensionless number to approximate the occurrence of the observed starvation condition (predominance of displacement flow):

$$SN = \frac{\eta_0 \cdot a \cdot f}{\sigma_s \cdot O_{SR}} \cdot \begin{cases} \frac{x}{2b} & \text{if } x \leq x_{SW}, \text{ regime 1} \\ \frac{x_{SW}}{2b} \cdot \frac{x_c - x}{x_c - x_{SW}} & \text{if } x_c \geq x > x_{SW}, \text{ regime 2} \\ 0 & \text{if } x > x_c, \text{ regime 3} \end{cases} \quad (1)$$

The number consists of two terms: A double amplitude-dependent term and a term representing the capillary-driven replenishing flow. The numerator of the latter part consists of the base oil viscosity η_0, half of the contact length perpendicular to the rolling direction a, and the oscillation frequency f since an increase in these values hinders the base oil reflow into the track. The opposite goes for the variables in the denominator, i.e., bleeding rate O_{SR} and the surface tension between the oil and air phase σ_s. To describe the mentioned amplitude effect, a second term depending on the amplitude, i.e., the travelled distance of the rolling element between the dead centres, x, is introduced. The travelled distance for the double amplitude at which the drop in wear initiation sets in is called x_{SW}. In the first regime below this threshold, the displaced volume per cycle increases with this distance. Above the limit, the number is modified in a manner that lowers the SN-number again. Wandel et al. explain the diminished wear initiation by relubrication through cage interaction. Finally, a further increase in amplitude, and therefore, the travelled distance x leads to the prevention of the measurable wear because relubrication by cage immersion effects dominates from this point onward. Correspondingly, there is an upper threshold $x > x_c$ implemented into the starvation number. To summarise, the SN-number can be interpreted as a ratio between the displacing and the replenishing flows around the contact. High values, therefore, lead to a higher risk of damage initiation. In a further publication, Wandel et al. [25] verify their proposed starvation number by testing three model greases with substantial differences regarding oil bleeding and base oil viscosity.

As Wandel et al. did previously, this paper focuses on $\frac{x}{2b}$ ratios greater than one and moderate frequencies from 0.2 to 5 Hz to be in a parameter range relevant to wind turbine blade bearings. They already proved experimentally that the proposed starvation number shows reliable results for different amplitudes, frequencies, and grease properties under small-scale laboratory conditions for point contacts. This investigation addresses the following issues regarding the work of Wandel et al.: validity for other bearing types, verification regarding the contact length $2a$, and scalability, especially to larger bearings. Therefore, experiments with CRTBs (designation 81212) with a considerably higher contact length $2a$ but of similar size (pitch diameter 77.5 mm) to the 7208, as well as significantly larger scaled blade bearings (SBB) with a pitch diameter of 673 mm are compared. Additionally, another small-scale ACBB type with the designation 7312 acc. to [22,23] (pitch diameter 95 mm) with a larger ball diameter (22.23 mm vs. 11.86 mm) is tested to obtain a larger data set. The general aim of the investigation is to fill the gap in the literature regarding the influence of double amplitude and frequency on the wear initiation and lubrication supply of grease-lubricated, highly loaded, oscillating rolling element bearings at slow maximum entrainment speeds. The investigations by Wandel et al. considered only one bearing type at a small geometric scale but provided a type of analysis that invites generalisation to larger scales and for other contact geometries. In the following, we consider these generalisations precisely to investigate whether the starvation number can be used more generally as a tool for large-scale blade bearings in wind turbines of different geometries.

2. Materials and Methods

This section describes the basic testing procedure, the bearing types tested and the associated test rigs, as well as the evaluation of the obtained measurement data. Figure 1 summarises the experimental procedure graphically. Since the experimental concept for all of the four tested bearing types is the same, a brief general description is given before a more detailed explanation of each test rig follows. In all conducted experiments, the inner ring of the bearing is subjected to a sinusoidal motion by a drive, while the outer ring is fixed. The bearing is stressed by a constant load and lubricated by a defined amount of fully formulated industrial grease. Due to the design of the test rig, two bearings are always tested simultaneously. Both bearings experience the same operating conditions and should produce the same torque and wear, but it is not possible to distinguish their results in the measurements from the test rig. For all experiments, the same grease with the properties listed in Table 1 was used. To mimic different operating conditions, the drive is capable of performing the sinusoidal motion of the inner ring with different frequencies f and double amplitudes φ. Both are kept constant during one test run. During the experiment, the rotation angle of the inner rings and the drive torque of the bearings are recorded by corresponding measurement devices. An experiment continues until a predefined number of oscillation periods is reached or until a critical drive torque is exceeded. Load and experimental parameters for all bearing types are shown in Table 2.

Table 1. Properties of the grease used for all experiments.

Property	Value
Thickener type	Lithium
Base oil type	synthetic
NLGI class	2
Kinematic base oil viscosity at 40 °C	50 $\frac{mm^2}{s}$
Oil seperation rate, acc. to [26] at 40 °C for 168 h	4%
Dropping point	>180 °C
Other	contains solid lubricants

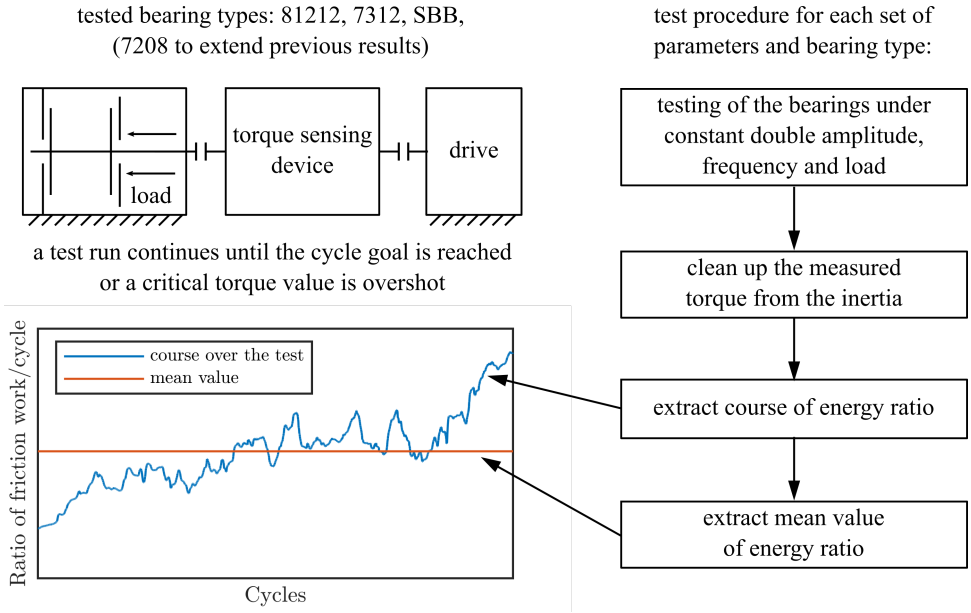

Figure 1. Workflow of the subsequent experimental investigation.

Table 2. Properties of the test rigs and bearings.

Property	7208	7312	SBB	81212
Bearing Type	ACBB	ACBB	2 row 4P BB	CRTB
Inner diameter	40 mm	60 mm	596 mm	65 mm
Outer diameter	80 mm	130 mm	750 mm	90 mm
Pitch diameter	60 mm	95 mm	673 mm	77.5 mm
Number of REs	14	12	2×69	3
Diameter RE	11.86 mm	22.23 mm	25.4 mm	11 mm
Contact length	3.2 mm	5.32 mm	6.59 mm	10 mm
Maximum contact pressure	2 GPa	2 GPa	2.5 GPa	2 GPa
Axial load	12.4 kN	25 kN	0	14.7 kN
Bending moment	0	0	150 kNm	0
Grease volume per bearing	10 mL	50 mL	600 mL	10 mL
Reduced moment of inertia	1.09×10^{-3} kgm^2	3.78×10^{-3} kgm^2	51.7 kgm^2	2.58×10^{-3} kgm^2
Goal cycle count	30,000	10,000	10,000	30,000
Brand of bearing manufacturer	FAG	FAG	IMO	INA

Point contacts on a small scale were tested by the use of ACBBs with the designation 7208 identical to WANDEL ET AL. to complement their experiments. The appointed test rig is described in more detail in their publication [21]. To compare between line and point contact, CRTBs with the designation 81212 were tested on the test rig depicted in Figure 2. Aside from the bearing unit itself, it is identical to the rig used for the 7208 bearings. A backlash-free-coupled servo motor subjects the bearings to sinusoidal oscillation. A torque measurement shaft between the motor and the shaft of the test unit records the inner ring rotation angle and torque. The test unit for the 81212 bearings is a modified version of the FE8 testing machine [27] and consists of two CRTBs as test objects and two radial support bearings that bear the weight of the shaft. The test bearings are centrally loaded with an axial force applied by compressing a set of disc springs under a hydraulic press. A load cell during pressing enables one to set the desired axial force. To test the 7312 bearings, the same test unit with different bearing supports is employed. The 7208, the 7312, and the 81212 bearings are all unsealed. The grease is applied on the raceways during assembly. Before applying the sinusoidal motion of the actual test to the small-scale bearings (7208, 7312, 81212), a short rotational run-in at 10 rpm takes place for two minutes to distribute the grease in the bearing. The maximum contact pressure in all small-sized bearings is

2 GPa. The relative measurement uncertainty of the torque measuring shaft is ±0.2% for the small-scale bearings.

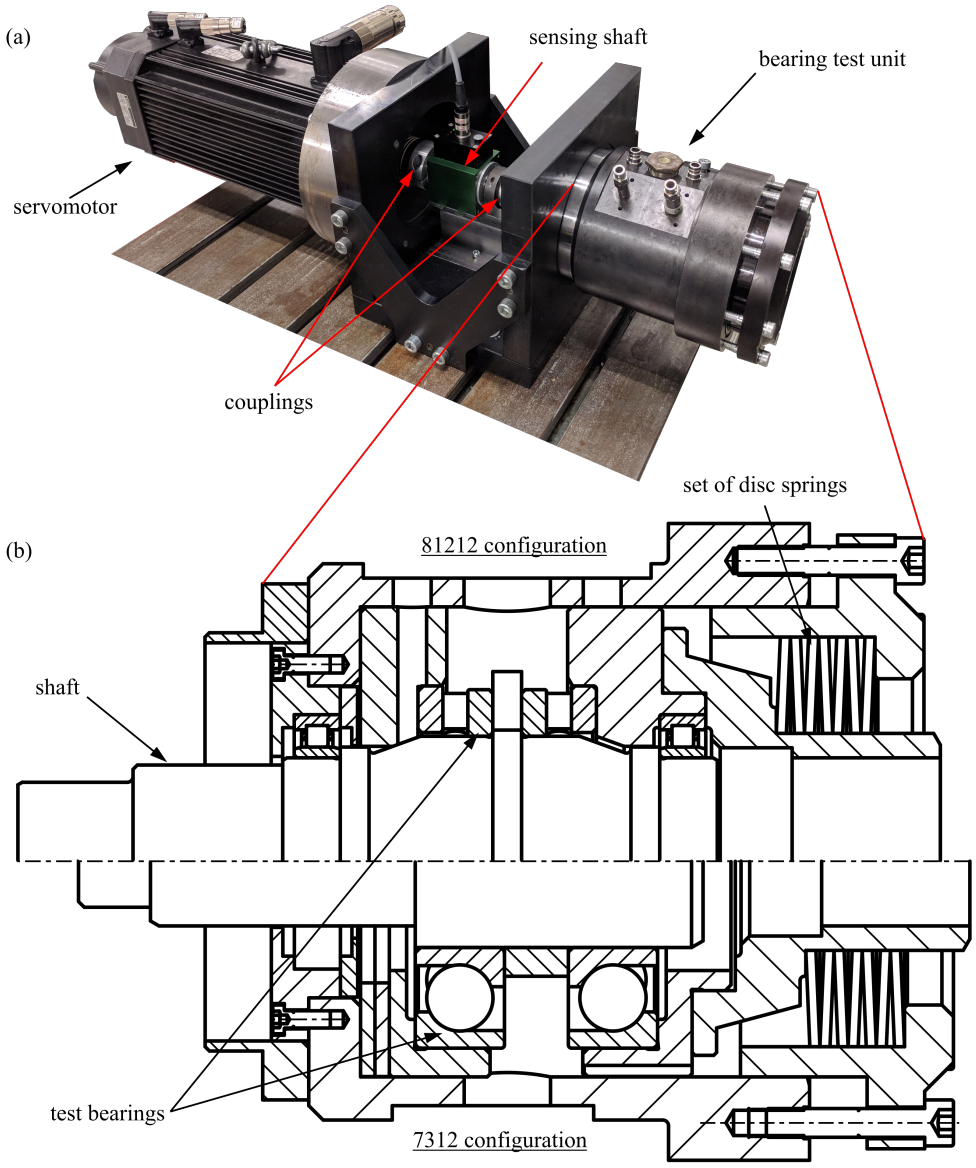

Figure 2. (**a**) Modified FE8 rig for testing grease-lubricated 81212 CRTB bearings under oscillating conditions; (**b**) section of modified FE8 test unit for 81212 (upper half) and 7312 (lower half) configuration.

The 4-point contact double-row bearings are tested on the BEAT1.1 (Bearing Endurance and Acceptance Test Rig 1.1) (see Figure 3). These bearings are smaller than modern blade bearings, but built with the same topology. In addition, the manufacturing processes are the same as for real-scale blade bearings. Hence, the surface finish, hardening processes and the overall stiffness of the bearings are comparable with real blade bearing applications. They also have a similar sealing technology to the large-scale bearings. Therefore, they are referred to as scaled blade bearings (SBB) in the following. The BEAT1.1 makes use of a hexapod construction and is able to apply loads at six degrees of freedom. Therefore, the design is particularly suitable for emulating load conditions that are typical for blade bearings of wind turbines. The test rig tests two bearings at the same time in back-to-back configuration. The inner rings of both bearings are coupled with a force-transmitting element, which also holds a gearing and is connected to an electrical pitch system. This system consists of a gearbox, a torque meter and an electric motor to enable the turning

movement of the bearings' inner rings. Thus, not only the torque of the bearings is measured but also the friction torque from the gearbox. To obtain measurements dedicated to the bearings, the measured torque has to be adjusted to eliminate the influence of the gearbox. A detailed description of this procedure is given in [28]. After assembling two test bearings to the test rig, each pair of bearings is tested with three different test programs to assess their individual friction torque properties. These test programs perform a total of 454 movements with $\pm 60^\circ$ at different speeds and load conditions. In addition to the friction torque evaluation of the undamaged bearings, these test programs are considered a suitable running in the procedure. Hence, the grease is properly distributed, and each segment of the raceways and each rolling element has undergone some overrollings before the wear-relevant cyclic test program with sinusoidal movements is applied to the bearings. In contrast to the experiments with the smaller bearings, a static bending moment is applied to the test bearings instead of a static axial force. The bending moment is set to M_y = 150 kNm, which leads to a maximum pressure of 2.5 GPa in the compression and traction sides of the bearing. The idea behind this test set-up is to achieve a nonuniform load distribution on the raceways to be able to study the influence of the contact pressure on the wear development. All information given with respect to the scaled blade bearings and oscillating movements will focus on the contact properties and ratios determined at the highest contact pressure.

Figure 3. BEAT1.1 test rig and 750 mm bearing ©Fraunhofer IWES/Ulrich Perrey.

To evaluate an experiment for a specific parameter combination of frequency f and double amplitude φ with regard to damage development and progression based on the frictional torque, the recorded measurement signal must still be processed. The recorded signal of the torque sensing devices T_{rec} from all test rigs can be split into several components:

$$T_{rec} = T + T_{acc}(\Phi) + T_{f,sup} \tag{2}$$

where T is the desired friction torque of the test bearings, and $T_{acc}(\Phi)$ is the acceleration torque due to the oscillating motion of the rotating parts dependent on the current angular position Φ. The friction torque of the potential support bearings of the test rig (only used for CRTB 81212) and other sources of friction not originating from the tested rolling contacts are summarised in $T_{f,sup}$. The acceleration torque can be obtained directly from the reduced moment of inertia of all rotating parts I_{red}, and the measured angular acceleration $\ddot{\Phi}$ if the torsional stiffness of the torque transferring components is negligible. The inertia I of the individual rotating parts is determined by a CAD-software and subsequently reduced to the speed of the inner ring according to the transmission ratios of the bearings. By

assuming the torque of the support bearing is negligible, the desired friction torque of the test bearings can be determined from the measured variables in this manner:

$$T = T_{rec} - I \cdot \ddot{\Phi} \tag{3}$$

By plotting the friction torque over the rotation angle for each period of the sinusoidal angle signal, one can obtain hysteresis loops such as in Figure 4a. A test run with n cycles will yield n hysteresis loops correspondingly. Since considering all loops for each experiment individually is cumbersome when it comes to comparing the results of different experiments, a more practical variable is desirable. The framed area of one hysteresis corresponds to the dissipated energy in one cycle. Since the goal of this investigation is to assess the influence of the oscillating parameters on the wear initiation and lubrication, the dissipated energy of one cycle is a suitable variable for evaluation. To make a comparison between different bearing types more accessible and to compensate for possible inaccuracy in applying loads, the values of the dissipated friction work/energy per cycle are normalised by the mean value of the dissipated energy of the first fifty cycles. An example of a plot of this energy ratio over the course of an experiment is shown in Figure 4b. To smoothen outliers, a running median with a window of twenty is applied to the energy ratio values of the small-scale bearings. For the SBB, a low-pass filter with a cutoff frequency of 25 Hz is applied to the torque measurements to cut out the influence of higher frequencies originating from the gearbox. The results for different oscillating conditions will be presented in the form of graphs of the friction work ratio.

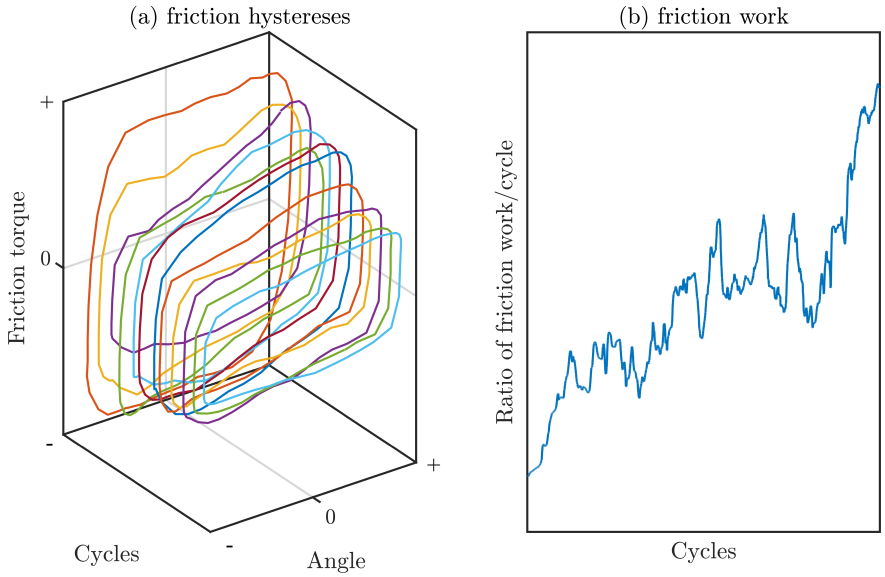

Figure 4. Example of obtained hysteresis loops.

The two parameters that can be altered to change the oscillation conditions for different test runs are the frequency f and the double amplitude φ. The ranges of each of these two parameters for the different bearing types used in the experiments are listed in Table 3. These test conditions were chosen to represent the oscillation conditions of interest stated in the introduction. For the 7208 type bearings, the experimental ranges are noticeably smaller since this bearing type was already extensively investigated by WANDEL ET AL., and the experiments conducted with these bearing types are just to supplement their results [21,25]. The test parameters given in Table 3 are partly dependent on each other. The $\frac{x}{2b}$ ratio and the double amplitude φ are linked by the contact geometry and the bearing kinematics. The second free parameter is the frequency f or maximum entrainment speed $v_{ent,max}$. The experimental design differs between the smaller bearings and the SBB in that, for the latter, the velocity and the double amplitude were used to define the experimental conditions,

whereas for the smaller bearings, the double amplitude and the frequency were used. The difference becomes clearer in the later evaluation of the experiments.

Table 3. Range of test parameters.

Property	7208	7312	SBB	81212
Frequency f	0.6–1 Hz	0.2–5 Hz	0.05–3 Hz	0.2–5 Hz
Double amplitude φ	11°	2–60°	0.75–7.5°	1–55°
$\frac{x}{2b}$-ratio	12.15	1.52–45.73	2.1–21	1–48.31
max. entrainment speed $v_{ent,max}$	7.24–12.06 $\frac{mm}{s}$	0.5–378.12 $\frac{mm}{s}$	3.5–20.7 $\frac{mm}{s}$	0.24–58.43 $\frac{mm}{s}$
Spanning of test space	f, φ	f, φ	$v_{ent,max}$, φ	f, φ

3. Results

3.1. Bearing Type 81212

Figure 5 shows the development of the energy ratio over 30,000 cycles for oscillation frequencies from 5 down to 0.2 Hz for an oscillation angle of 11°. The tests with 1 and 5 Hz almost immediately show a steep incline of the energy ratio and therefore also the general torque level. To protect the torque sensing shaft from high oscillating loads, the runs are aborted before the cycle goal of 30,000 cycles is reached. After 9000 cycles each, the experiments at 1 and 5 Hz show an energy ratio above four, i.e., the dissipated energy of one cycle quadrupled in comparison to the average of the first fifty cycles. For 0.6 Hz, the energy ratio seems to reach a quasi-steady state at a ratio of 2.5 with peaks up to 3 and minimums of 2. For 0.4 Hz, the ratio first rises to a maximum value of 1.5 and then starts to drop in the remaining cycles to a magnitude of approximately 1. Compared to the previous higher frequencies, the energy ratio shows fewer fluctuations in the course of the experiment. For an oscillation frequency of 0.2 Hz, there is no visible change in the ratio; it stays close to unity and experiences few fluctuations compared to the previous runs.

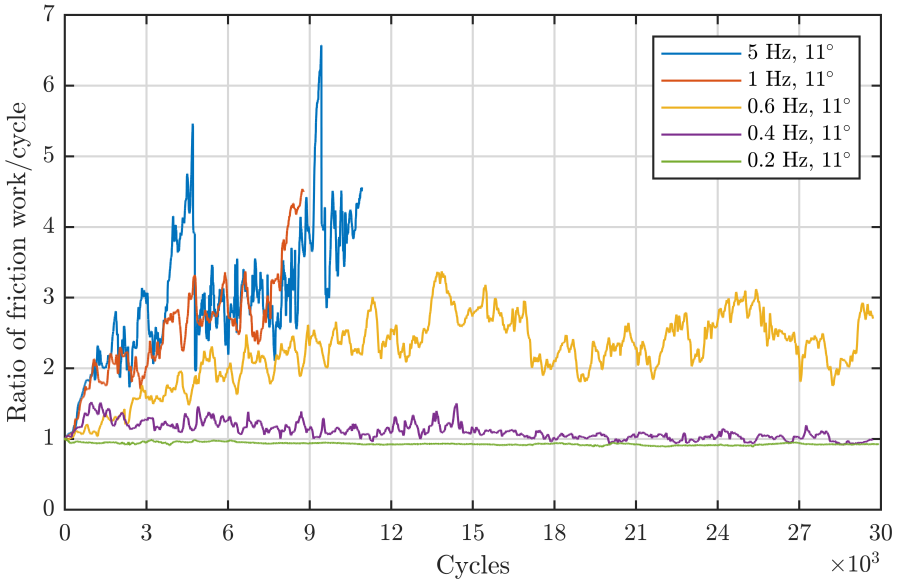

Figure 5. Frequency influence for type 81212 bearings at a double amplitude of 11°.

For repeatability, the experiments at 0.2 and 0.4 Hz were repeated and are shown in Figure 6 with a zoom-in on the ordinate. The repetitions are comparable to the first runs. There is a clear difference in the ratios between the two frequencies.

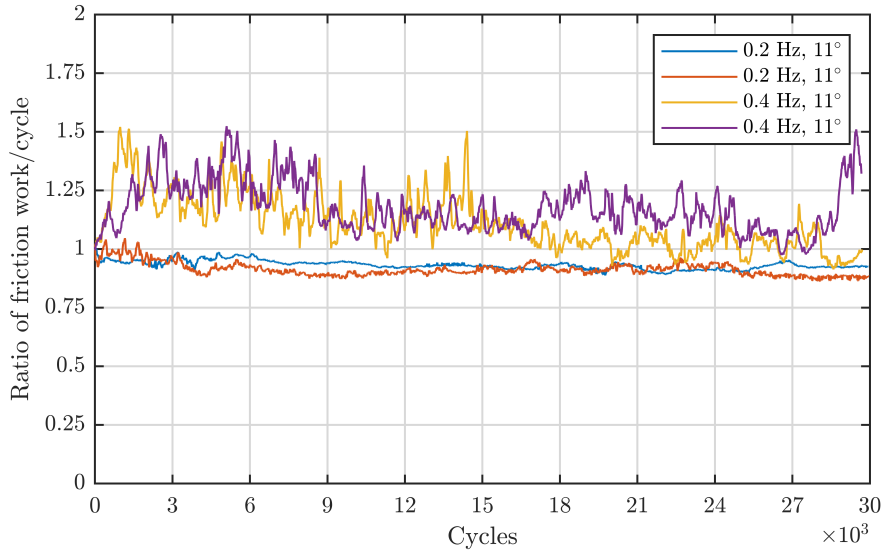

Figure 6. Repeatability tests with type 81212 bearings at 11° and 0.2 Hz/0.4 Hz.

The response of the energy ratio to different double amplitudes for type 81212 bearings at a constant frequency of 1 Hz is shown in Figure 7 for angles below 11° and in Figure 8 for angles above 11°. Starting with a double amplitude of 1° and a frequency of 1 Hz, the dissipated energy ratio stays at one during the whole course of the test. Increasing the double amplitude to 6° causes an energy ratio with more fluctuations and a rise to a maximum of 1.5. A further increase in double amplitude to 9° yields a highly fluctuating signal with a distinctive rise in energy ratio up to 4 before the run was stopped. The run under 11° was already described in the context of Figure 5. Figure 8 displays the energy ratio at a frequency of 1 Hz for different double amplitudes from 11° to 55°. With an increasing amplitude from 11° onwards, the ratio decreases again. For 25°, the ratio reaches a value of around 2 at the end of the run, although it shows comparably high fluctuations. With an amplitude of 35° and 55°, the ratio stays close to one. The latter one has a much smoother appearance.

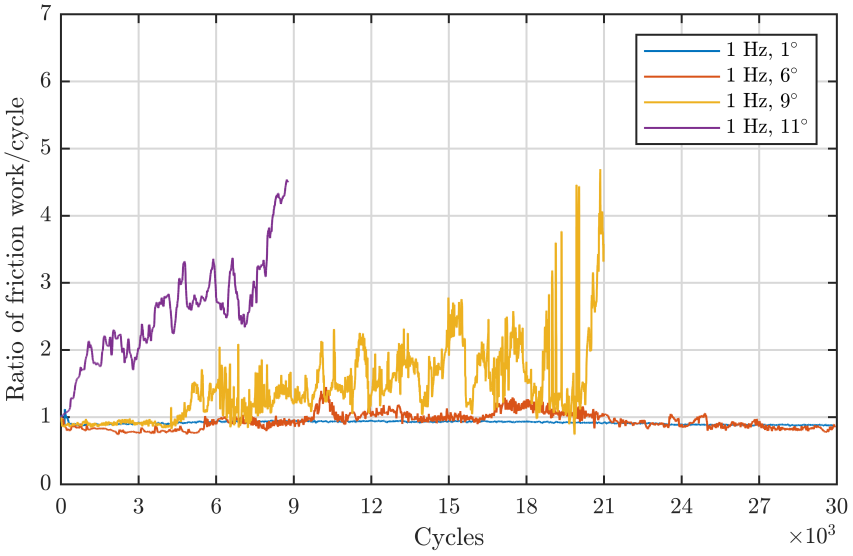

Figure 7. Angle influence below 11° for type 81212 bearings at a frequency of 1 Hz.

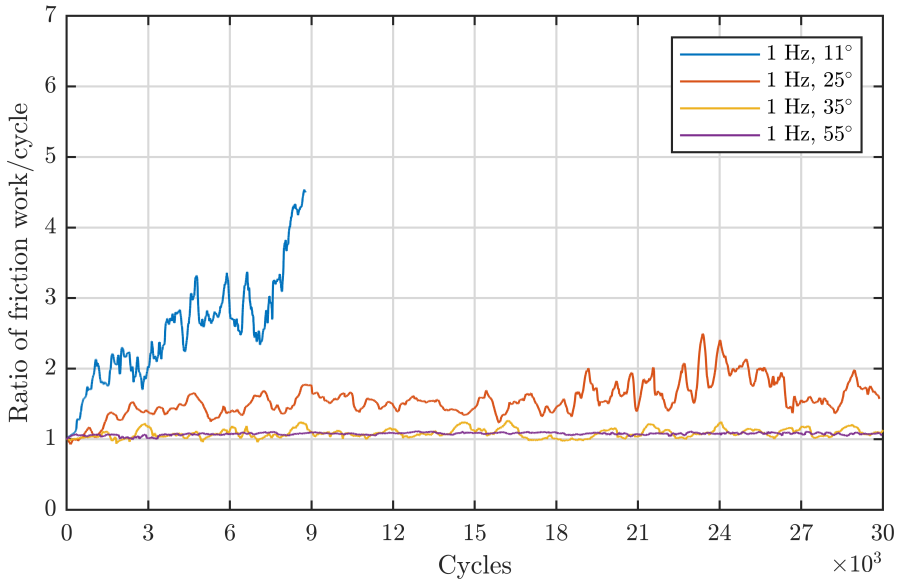

Figure 8. Angle influence above 11° for type 81212 bearings at a frequency of 1 Hz.

3.2. Bearing Type 7208

To compare the results of the 81212 bearings regarding the oscillation frequency in light of the sensitivity of the starvation number to the contact length, the experiments with point contacts of Wandel et al. [21,25] have been complemented by the results shown in Figure 9. With the additional experiments, the range between 0.2 and 1 Hz is supported by more data. The angle of 15° corresponds to a similar $\frac{x}{2b}$ ratio as for the 11° of the 81212 type bearings. The experiment with 1 Hz was taken from [21] since the therein mentioned Grease 1 corresponds to the grease used in this investigation. For 1 Hz and 15°, the energy ratio followed a steep incline before the test run was shut off after 4000 cycles with an energy ratio of five. Wandel et al. conducted their experiments with a lower cycle goal of 4000. For 0.8 Hz and the same double amplitude, the torque ratio is nearly one for the whole experiment and does not exhibit major fluctuations in the signal. The same applies to the test with 0.6 Hz and 15°.

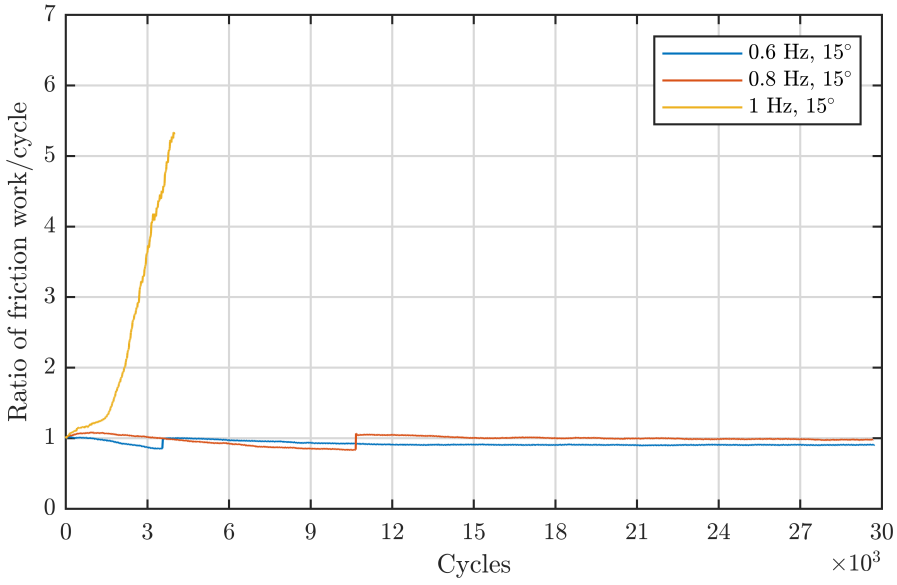

Figure 9. Frequency influence for type 7208 bearings at a double amplitude of 15°.

3.3. Bearing Type 7312

The experimental results of the bearing type 7312 can be found in the Appendix A in Figures A1–A5. They are not described in detail since they do not exhibit a new distinctive feature compared to the 7208 bearings of WANDEL ET AL. except their larger ball diameter. Nevertheless, they are interesting for the broader evaluation, following in the next chapter, to obtain a larger amount of data for validation.

3.4. Scaled Blade Bearings

After the results of the smaller standard 81212 and 7208 bearings, the considerably larger, downscaled blade bearings follow. The testing series of the smaller bearings and the downscaled blade bearings were not synchronised from the beginning on. Therefore, a different method of spanning the space of testing parameters was employed. Instead of using the double amplitude of the inner ring angle and the frequency, the double amplitude and the maximum entrainment speed during the oscillation cycle were used. This results in three plots (Figures 10–12) showing the energy ratio under different double amplitudes for constant entrainment speeds. Starting with a constant entrainment speed of 3.5 $\frac{\text{mm}}{\text{s}}$ in Figure 10 and the lowest angle of 0.75°, the energy ratio starts to rise immediately. After 4000 cycles, the increase becomes much flatter and levels off at around 1.7 towards the end of the 10,000 cycles. For the same entrainment speed but with a double amplitude of 1.5°, the behaviour is nearly similar, with the only difference being that the energy ratio slowly descends onto 1.55 at the end after reaching its maximum at 4000 cycles. For 2.25°, the course is similar to 1.5° but the peak of about 1.9 is a bit higher. The last two double amplitudes of 3.75° and 7.5° show less fluctuation in the energy ratio compared to the previous graphs. For 3.75°, the energy ratio starts around one and rises slightly over the cycle count and finally reaches a maximum of about 1.05 at the end of the test. A similar trend applies for the maximum double amplitude of 7.5°. Hence, both energy ratios stay close to one during the course of the test.

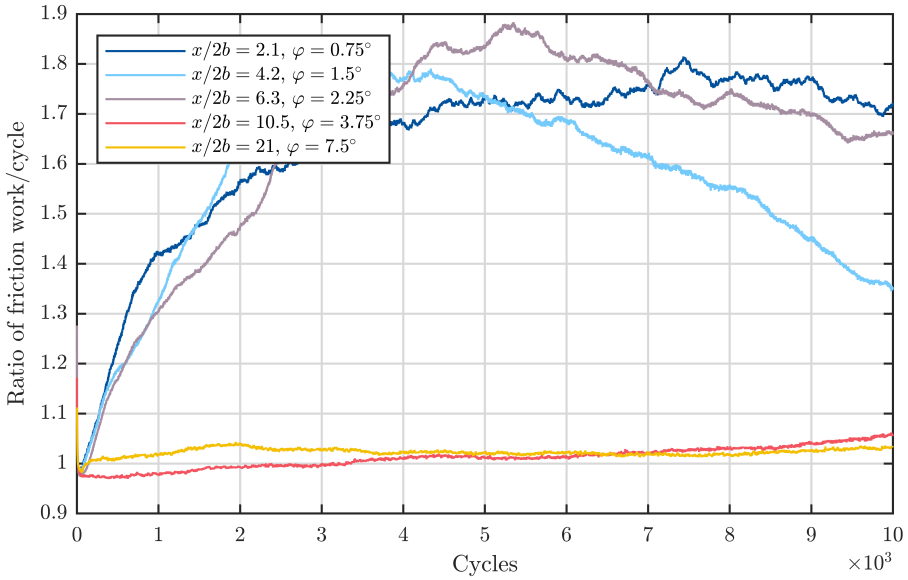

Figure 10. Angle influence for SBB at an entrainment speed of 3.5 $\frac{\text{mm}}{\text{s}}$.

Figure 11 shows the energy ratio for different double amplitudes in the same fashion for a maximum entrainment speed of 10.4 $\frac{\text{mm}}{\text{s}}$. For a double amplitude of 0.75° the energy ratio rises similarly as before for 3.5 $\frac{\text{mm}}{\text{s}}$ but reaches a plateau of about 2.8. For the double amplitude of 1.5°, the ratio rises to a peak value of 3.2 at 7000 cycles and lowers to 2.5 until the end of the experiment. The following experiment for a double amplitude of 2.25° ends at a ratio of 2.75, whereas for 3°, the dissipated energy ratio rises only to a peak of 2.4 and declines towards the end of the test to 1.9. The trend continues for a double amplitude of

3.75° and so only a maximum of 1.6 is reached. Similar to the slower entrainment speed in Figure 10, the energy ratio stays nearly constant at one for the highest double amplitude of 7.5°.

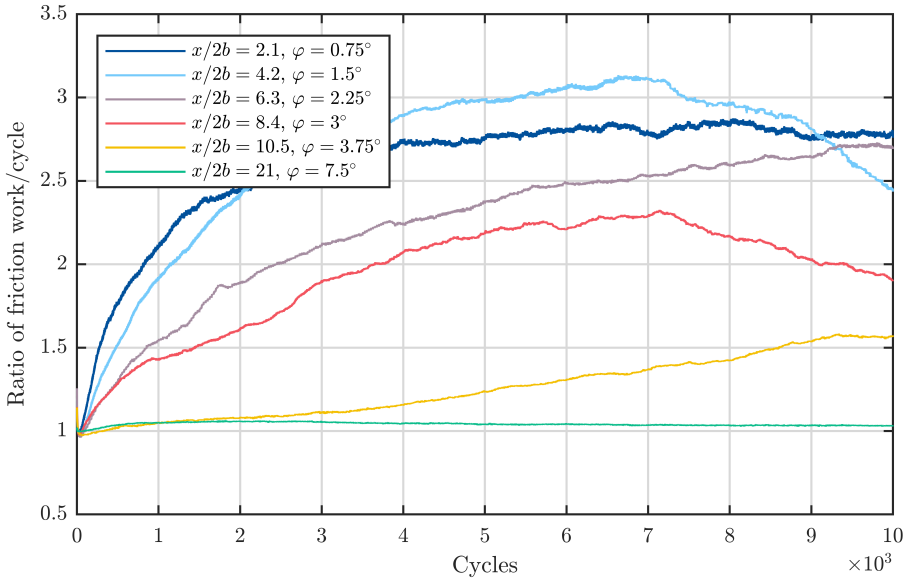

Figure 11. Angle influence for SBB at an entrainment speed of 10.4 $\frac{\text{mm}}{\text{s}}$.

Finally, Figure 12 shows the results of the test runs with the highest maximum entrainment speed of 20.7 $\frac{\text{mm}}{\text{s}}$. The double amplitudes of 0.75°, 1.5° and 2.25° all reach maxima above two, although they are a bit lower compared to the values for 10.4 $\frac{\text{mm}}{\text{s}}$. Again the graph for a double amplitude of 3.75° is noticeably lower with its maximum of 1.75. Finally, the energy ratio for the double amplitude of 7.5° only shows a moderate increase to 1.1 over the first 2000 cycles and stays constant for the rest of the test.

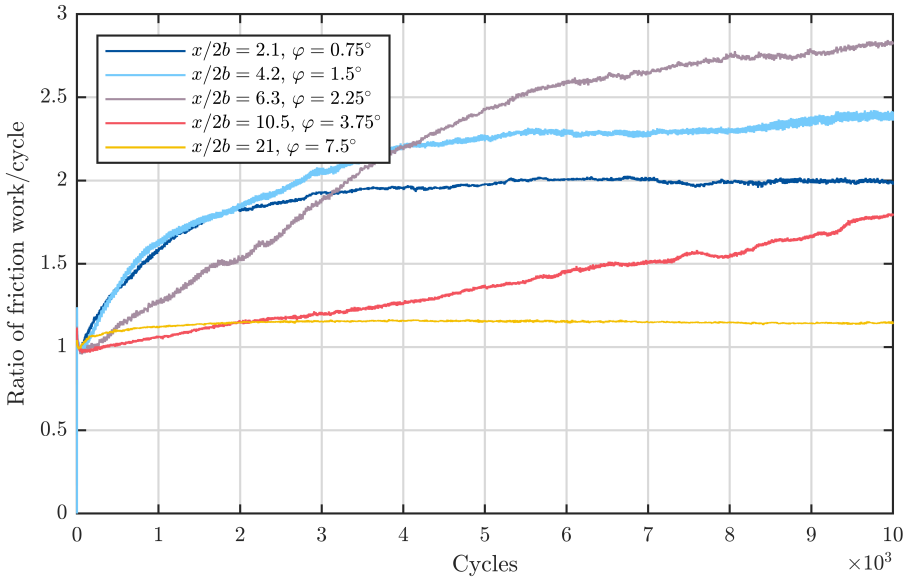

Figure 12. Angle influence for SBB at an entrainment speed of 20.7 $\frac{\text{mm}}{\text{s}}$.

3.5. Visual Appearance of Bearing Surfaces

Figure 13 shows the condition of the 81212 CRTB washers after the test. As an example, the washers corresponding to Figure 5 with a double amplitude of 11° are shown. For all parameters except a double amplitude of 11° and 0.2 Hz, damage in the form of red

oxides and surface craters is visible. The extent of the damages appears to decrease with lower frequencies.

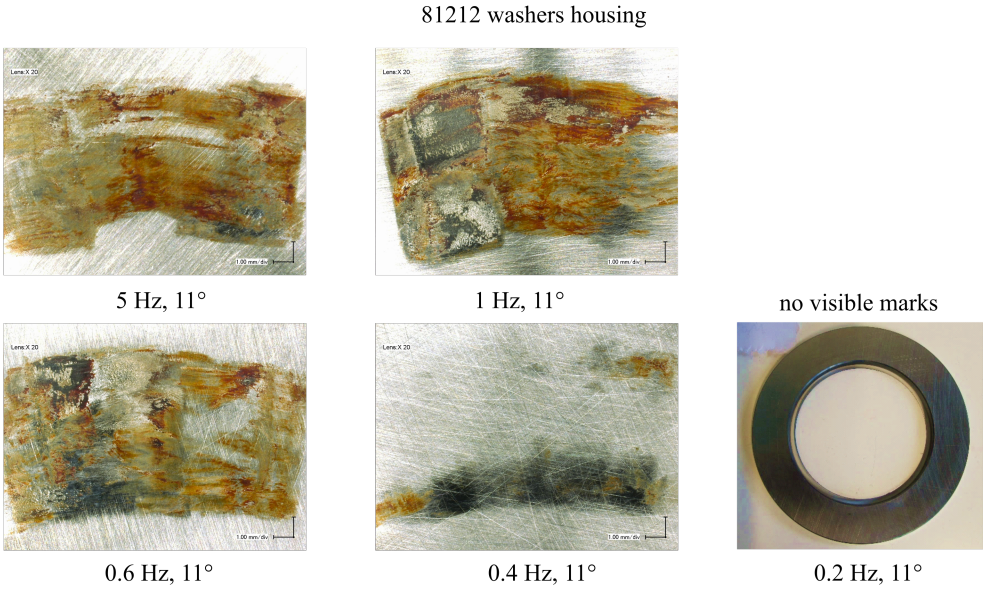

Figure 13. Damage marks for type 81212 bearings.

Figure 14 shows images of wear marks on the scaled blade bearing raceways for a double amplitude of 2.25° and increasing frequency. The images are taken from wear marks located in the highest loaded areas of the bearings. For all test conditions, wear is clearly visible. With increasing frequency, the wear marks appear shinier and show fewer signs of tribo-corrosion (red oxides) and micropittings, which could be an indicator of a faster wear progression throughout the test, as abrasive wear mechanisms seem to lead to a more polished appearance.

Figure 14. Damage marks for SBB at different test parameters.

4. Discussion

First, the suitability of the friction torque as an indicator for wear initiation is discussed. Second, the validity of the results from Wandel et al. [21,25] for the new bearing types and size is addressed using the experimental results. Third, the starvation number is applied to the tested bearings and analysed for validity.

Becker already showed that there is a strong correlation between the friction torque and the formation of wear marks in oscillating bearings. There was a nearly linear relation between the maximum wear depth and the rise in friction torque in his results [14]. The investigations of Wandel et al. show similar results just by optical comparison: the more pronounced the damage mark, the higher their observed torque rise. Aside from elastical compression and decompression that may occur when a rolling element enters or leaves

a damage indent, the torque signal is mainly composed of friction forces in the contact. Therefore, the relation between wear marks and friction should also apply to the dissipated energy. This is fully confirmed by the experiments conducted in this study, as can be seen by comparing the dissipated energy ratios of the 81212 bearings and the SBB with their corresponding damage marks (Figures 13 and 14). Since the energy ratio is apparently a reliable indicator of the extent of the wear, the discussion will be solely based on it. To enable a direct comparison between different bearing types, the energy ratio that puts the dissipated energy of one cycle into relation with the average dissipated energy of the first 50 cycles is used. The rise of the friction torque and dissipated energy can be attributed to the apparent lack of lubricant and therefore adhesive and abrasive wear mechanisms in the contacts.

In the following, the results are discussed in light of the findings from Wandel et al. regarding the influence of the oscillation double amplitude and the $\frac{x}{2b}$-ratio [21,25], respectively. From their findings, they deduce that there are three distinctive regimes of the $\frac{x}{2b}$-ratio. In the first regime, an increase in the $\frac{x}{2b}$-ratio in conjunction with a constant oscillation frequency leads to more severe wear development. After a certain threshold, the second regime begins and the opposite relation is the case; damage becomes less pronounced with a further increase in the ratio. Finally, in the third regime, wear is not encountered anymore. This behaviour can be explained in the context of their concept of two counteracting flows, namely the displacement flow of lubricant out of the track by the rolling element and the replenishing flow into the track induced by capillary forces. It is likely that the replenishing flow induced by surface forces mostly takes place in the vicinity of the contact and not at the free surface far away from the contact [29]. Since the replenishing flow is of a diffusive type, the volume of base oil that is able to replenish the track is dependent on the duration of one cycle, i.e., the frequency. While keeping the frequency constant, the amount of replenished base oil per cycle should not be severely affected by changes in the double amplitude. Contrary to this, the displaced base oil amount per cycle depends directly on the travelled distance x of the rolling body. Therefore, while increasing the $\frac{x}{2b}$-ratio at a constant load and frequency, the balance of flows shifts in favour of the displacement flow, and the contact is more likely to run dry and be more prone to wear. Wandel et al. observed the torque rise with increasing $\frac{x}{2b}$-ratios in their experiments until the aforementioned threshold in form of the second regime is reached. They argue that the following decline in torque, and ultimately, the absence of wear due to the increase in double amplitude is linked to the activation of further lubrication transport mechanisms into the contact area. They suspect the immersion of the rolling element surface into the grease-filled pockets of the cage as the major mechanism behind these secondary lubrication mechanisms. A significant effect of the cage for rotating grease-lubricated bearings was already reported by Damines et al. They observed higher film thicknesses with reduced cage clearance and argued that the higher films are due to an enhanced redistribution of the grease onto the tracks for smaller clearings. Furthermore, increased sheer degeneration can possibly contribute [30].

Assessing the response of the energy ratios from the 81212 bearings to an increasing angle can be performed by looking at Figures 7 and 8. Both confirm the observed regimes of Wandel et al. Figure 7 comprises angles that are located in the first regime: an increase in angle at a constant frequency leads to more severe damage. Figure 8 depicts the second and third regime: increasing the double amplitude from 11° onwards while keeping the frequency constant at 1 Hz leads to continuously lower energy ratios. From this standpoint, the observed double amplitude behaviour from Wandel et al. also seems to be valid for line contacts in the same dimension. To validate this also for the larger-sized, downscaled blade bearings, a less direct approach is necessary since there is no directly comparable data with a constant frequency due to the different underlying design of the experiments. Since for these experiments the maximum entrainment velocity was kept constant, an increasing $\frac{x}{2b}$ ratio results in a decreasing oscillation frequency. This hinders a direct comparison between the frequency-angle-based and the velocity-angle-based testing approach. Therefore, in

the following, the starvation number from Equation (1) is converted into a velocity-based formulation. For a given double amplitude φ and a frequency f, the maximum (max) inner ring (i) angular velocity in an absolute coordinate system for a sinusoidal motion of the inner ring is:

$$\omega_{i,max} = f \cdot \varphi \cdot \pi \tag{4}$$

For a bearing with a fixed outer ring in an absolute coordinate system, the inner ring angular velocity in a cage-fixed relative system can be expressed as [31]:

$$\omega^*_{i,max} = f \cdot \varphi \cdot \pi \cdot (\frac{1}{2} + \lambda) \tag{5}$$

The factor λ describes the ratio between the rolling element radius R projected into the plane perpendicular to the bearing main axis and the pitch diameter r_p of the bearing. For a given contact angle α it is: $\lambda = \frac{cos(\alpha) \cdot R}{r_p}$. The maximum entrainment speed under the observed conditions $v_{ent,max}$ can therefore be expressed as:

$$v_{ent,max} = f \cdot \varphi \cdot \pi \cdot (\frac{1}{2} + \lambda) \cdot (r_p - cos(\alpha) \cdot R) \tag{6}$$

To insert Equation (6) into the starvation number, it is desirable to substitute the double amplitude by the $\frac{x}{2b}$ ratio. By integrating the absolute value of Equation (6) over half a period, one can obtain the following relation between x and the double amplitude φ:

$$\frac{x}{2b} = \frac{\varphi \cdot (\frac{1}{2} + \lambda) \cdot (r_p - cos(\alpha) \cdot R)}{2b} \tag{7}$$

Therefore, the product $f \cdot \frac{x}{2b}$ can be put into a form dependent only on $v_{ent,max}$ and $2b$: $f \cdot \frac{x}{2b} = \frac{v_{ent,max}}{2b \cdot \pi}$. Hence, the starvation number can be transformed into a version depending on the maximum entrainment speed:

$$SN = \frac{\eta_0}{\sigma_s \cdot O_{SR}} \cdot a \cdot \begin{cases} \frac{v_{ent,max}}{2b \cdot \pi} & \text{if } x \leq x_{SW} \\ \frac{v_{ent,max}}{2b \cdot \pi} \cdot \frac{\frac{x_c}{x} - 1}{\frac{x_c}{x_{SW}} - 1} & \text{if } x_c \geq x > x_{SW} \\ 0 & \text{if } x > x_c \end{cases} \tag{8}$$

According to Equation (8), a constant maximum entrainment velocity, such as in the downscaled blade bearing experiments, corresponds to a constant risk of the contact running dry and therefore also damage initiation in the first regime. In this form, Figures 10–12 are more clear with regard to the angle behaviour described by the oscillating grease starvation theory by Wandel et al. Starting with $v_{ent,max} = 3.5 \frac{mm}{s}$ in Figure 10, the graphs for the first three double amplitudes 0.75°, 1.5°, and 2.25° are nearly the same. This complies with the starvation number for a constant entrainment velocity (Equation (8)) and indicates that these three double amplitudes/$\frac{x}{2b}$ ratios lie within the first regime. For the two remaining amplitudes of 3.75° and 7.5° in Figure 10, the friction energy ratio stays as one throughout the course of the experiment, although the entrainment speed remains constant. This can be explained by the second or third regime of the starvation number, which is numerically represented by lower values or zeros in these regimes. Physically spoken, these values greater than x_c are believed to correspond to an immersion of the rolling element into grease reservoirs present close to the pockets of the cage. Hence, there is the possibility of grease and base oil being dragged into the contact and thus preventing damage initiation.

Looking at the greater entrainment velocity of $v_{ent,max} = 10.4 \frac{mm}{s}$ in Figure 11, generally higher values of the energy ratio are visible. This corresponds to a higher starvation number due the increased speed (see Equation (8)). The previous observation of nearly

identical energy ratio curves for low double amplitudes does also apply in this case. For the double amplitudes of 0.75°, 1.5°, and 2.25°, the curves of the energy ratio are similar. Therefore, these double amplitudes can be located in the first regime. The double amplitudes 3° and 3.75° exhibit lower levels and therefore belong in the second regime. For a speed of $v_{ent,max} = 3.5\,\frac{\mathrm{mm}}{\mathrm{s}}$, the double amplitude of 3.75° did not exhibit any friction energy rise. This can be explained by the rise in velocity and, therefore, also starvation risk by means of the starvation number in the second regime. Again for a double amplitude of 7.5° there is no rise in the torque signal, which supports that this amplitude is located in the third regime. For the highest entrainment velocity of $v_{ent,max} = 20.7\,\frac{\mathrm{mm}}{\mathrm{s}}$, the findings of $v_{ent,max} = 10.4\,\frac{\mathrm{mm}}{\mathrm{s}}$ are generally confirmed. The only discrepancy is that the energy ratios in the first regime are a bit lower than for the previously discussed speed of $v_{ent,max} = 10.4\,\frac{\mathrm{mm}}{\mathrm{s}}$. It should be mentioned that the starvation number is primarily intended to predict the general occurrence of starvation and therefore also rise in friction energy. However, the magnitude of the friction energy over the cycles is also dependent on the wear development involving possibly more factors. However, the starvation theory presented by Wandel et al. showed good performance in explaining the results of the SBB and 81212 with respect to the influence of the double amplitude φ. A direct comparison with further literature is difficult since there are no other known studies incorporating torque measurements in combination with a systematic variation of the double amplitude. Phaner-Goutorbe et al. could not find a direct difference in the wear progression with double amplitudes ranging from 3° to 12° [12]. Their judgement was based on surface changes only under consideration of significantly higher frequencies of up to 20 Hz. A broader evaluation of the test is not available. Furthermore, a direct link between the change in surface roughness and friction torque is not reasonable, as can be seen by Wandel et al. [32]. After the initiation of damage by a lack of lubricant, several wear mechanisms can occur in succession. If after a first adhesive phase, abrasion sets in, the surface roughness will even decrease again, even though a significant rise in friction torque occurred. For this reason also, the results of Maruyama et al. are not directly comparable to this investigation, although they show the same behaviour regarding the double amplitude in the first regime with their low-viscosity base oil grease [13].

After the influence of the double amplitude, i.e., the $\frac{x}{2b}$ ratio, was discussed, the discussion of the frequency followed. Wandel et al. observed a continuous increase in damage development and torque rise if the frequency was increased for a constant double amplitude [21,25]. Figure 5 confirms this for the 81212 bearings. For a double amplitude of 11°, the critical frequency f_c that first leads to damage initiation seems to be between 0.2 and 0.4 Hz. For comparison between point and line contacts, the experiments of Wandel et al. with 7208 bearings have been complemented by the results in Figure 9. In this case, the critical frequency lies between 0.8 and 1 Hz. The critical frequencies for the given $\frac{x}{2b}$ ratios are estimated by the mean value of the corresponding borders given in Table 4. For the line contact of the 81212 bearing, the critical frequency is three times higher than for the point contact of the 7208 bearings. This finding is in good accordance with the starvation number by Wandel et al. since the longer contact length hinders a fast replenishment of the area around the rolling element. To evaluate the numerical accuracy of the starvation number, the same critical starvation number is assumed for both bearings. Since the same grease was used and both angles lay within the first regime, Equation (1) yields:

$$\frac{f_{c_{81212}}}{f_{c_{7208}}} = \frac{\frac{x}{2b}_{81212} \cdot a_{81212}}{\frac{x}{2b}_{7208} \cdot a_{7208}} \tag{9}$$

This ratio of the critical frequencies calculated based on the contact geometry is 2.8 and therefore in good accordance with the experimentally determined ratio of 3. For this example, the starvation number of Wandel et al. seems to perform satisfactorily for line contacts. Before a more comprehensive analysis of the predictive capabilities of the number is performed, the frequency-sensitivity of the SBB is discussed.

To assess the influence of the frequency for the SBB, tests with the same double amplitude in Figures 10–12 are compared. Since the entrainment speed is increasing for each of these figures and fixed double amplitudes are compared, the frequency is increasing for the following way of comparing. Starting with a double amplitude of 0.75°, it can be observed that the increase in frequency by changing the entrainment speed from $v_{ent,max} = 3.5 \frac{\text{mm}}{\text{s}}$ to $10.4 \frac{\text{mm}}{\text{s}}$ leads to an increase in the energy ratio maximum from 1.8 to 2.8. This increase is in agreement with the observations from the smaller 7208 and 81212 bearings. Contradicting this, a further increase in the speed to $v_{ent,max} = 20.7 \frac{\text{mm}}{\text{s}}$ brings a lower maximum of 2. The remaining double amplitudes in the first regime, 1.5° and 2.25°, show a similar trend. As mentioned, the starvation number is mainly intended to assess the general occurrence of wear and not so much the wear progress. This indicates that there might be a speed-dependant influence in the wear progression. At a double amplitude of 3.75° that is suspected to lay in the second regime, the maximum value of the energy ratio increases slightly when increasing the speed from $10.4 \frac{\text{mm}}{\text{s}}$ to $20.7 \frac{\text{mm}}{\text{s}}$. For a double amplitude of 7.5° there is no difference between the discussed speeds since the double amplitude lays within the third regime where damage does not arise any more. Again, a comparison to Phaner-Goutorbe et al. and Maruyama et al. is not possible since torque values were not measured in their investigations [12,13].

Table 4. Comparison of critical frequencies between small-scale 7208 and 81212 bearings.

Bearing Type	**81212**	**7208**
Double amplitude	11°	15°
Experimentally determined critical frequency	0.3 Hz	0.9 Hz
Contact length perpendicular to rolling direction	10 mm	3.2 mm
Ratio $\frac{x}{2b} \cdot a$	2.8	
Ratio of f_{crit}	3	

In summary, the presented results for the investigated bearing types agree with the results by Wandel et al. regarding the wear initiation in dependency of the double amplitude and oscillation frequency [21,25]. They summarised their work in "colourmaps" that show the frequency on the abscissa, the double amplitude on the ordinate, and represented torque using a colour scale. Figure 15 uses the same concept to summarise the results for the SBB (a) and the 81212 bearings (b), but instead of using the maximum torque, the average energy ratio of the test is used. In further contrast to the maps of Wandel et al., not the whole grid shown in the maps was covered by experiments. Hence, the data for the maps were obtained by linear regression for a constant double amplitude and subsequent linear interpolation between this regression data for a constant frequency. For the 81212 bearings, additional experiments were completed near the critical starvation number to have a larger amount of data. The parameters of the additional experiments are given in Table A1. For the SBB, the lines of constant speed are indicated as well. The maps confirm the previous discussion of the results and show the different regimes of the double amplitude and the frequency influence.

For a more quantitative analysis, the starvation numbers SN for the SBB, the 81212 bearings and the additionally tested 7312 bearings were calculated. To determine the x-thresholds of the second and third regime, the highest and the lowest value of the regimes identified by the energy ratio were used (details in Table A2). In Figure 16, the mean value of the energy ratio for each test is plotted over the calculated starvation numbers (1 was added to the SN to enable logarithmic scaling). For reference, the 7208 tests of Wandel et al. with the same grease as used here are also included. Although there is some scatter in the data, it is noticeable that most of the experiments with low energy ratios also show low starvation numbers and vice versa. By defining a critical energy ratio of 1.4, i.e., to tolerate a maximum increase in friction energy by 40%, and assuming a critical starvation number of $SN_{crit} = 1$, a classification error of 22% is obtained. Table 5 shows the corresponding data. In Figure 17 this critical starvation number is used to classify all the

experiments and show the results again in the form of a boxplot. Although there are some outliers for SN-values below the critical limit that show an energy ratio in the magnitude of two, the general performance is satisfying especially when fluctuations typical of grease-lubrication are considered. It shows that the oscillating grease starvation number proposed by Wandel et al. [21,25] based on experiments with only one small-scale bearing type and different greases also seems to be a valid tool to detect possible wear in critical operation conditions also for different contact geometries and larger bearings.

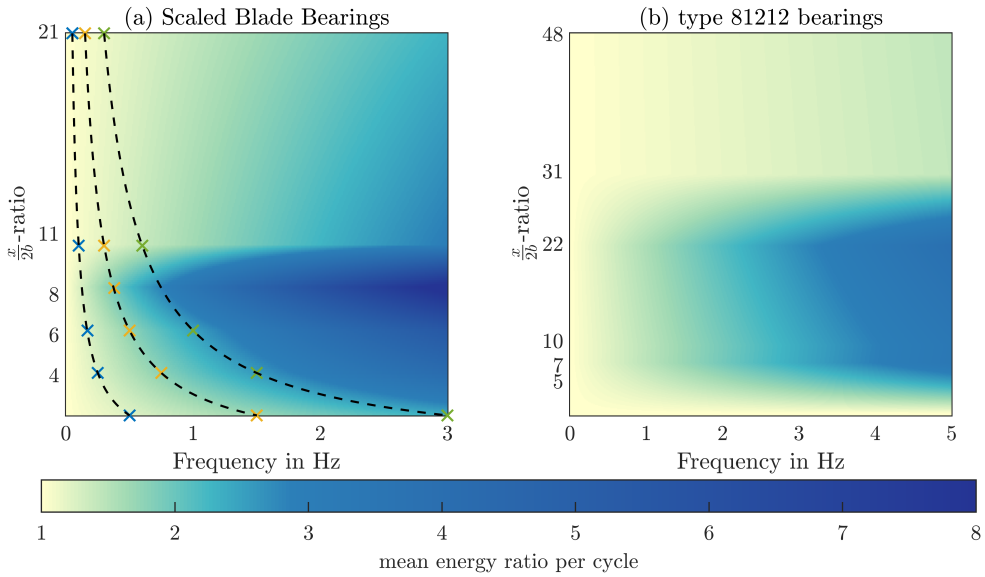

Figure 15. Colourmap of mean dissipated energy ratio for (**a**) SBB (including lines of constant maximum tangential velocities) and (**b**) 81212 bearings.

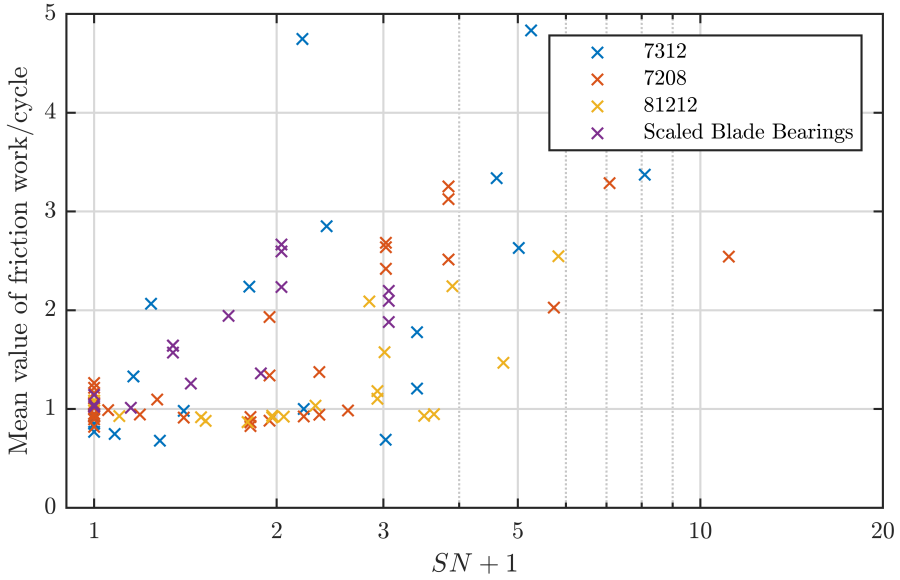

Figure 16. Dependency of wear initiation on the oscillating starvation number for all tested bearings.

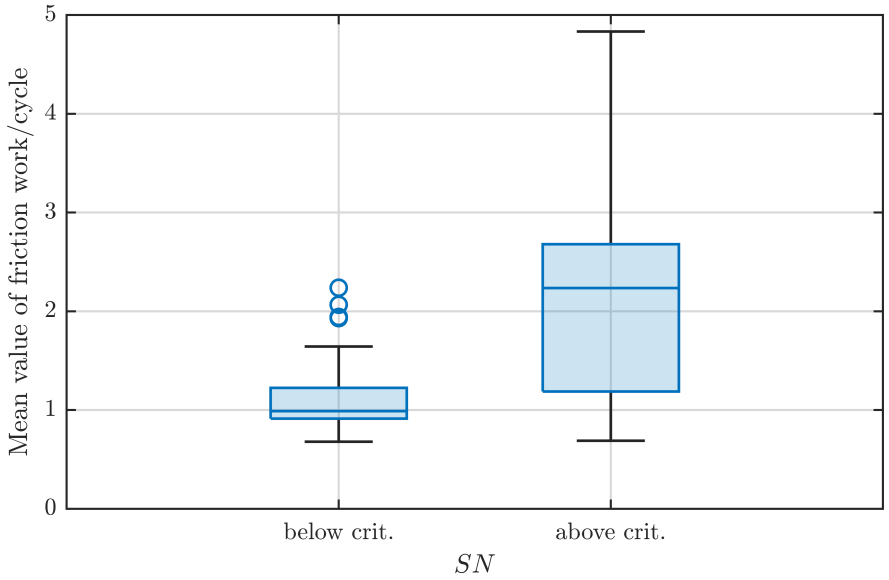

Figure 17. Box plot of average dissipated energy per cycle for low and high SN number.

Table 5. Classification of experiments based on a critical mean energy ratio of 1.4 and a critical starvation number of 1.

	***SN*-Low**	***SN*-High**
low mean energy ratio	42	13
high mean energy ratio	7	30

A closer look at Equation (8) reveals that the SN number is a kind of capillary number, as it is often used to characterise flows dominated by surface tension. Although there is a variety of these numbers, a basic form that puts the viscous forces into relation to the surface tension σ_s reads: $Ca = \frac{\eta v}{\sigma_s}$ [33]. The viscous forces are represented by the product of dynamic viscosity η and speed v responsible for the shear in the fluid. The Ca number can be used to formulate the starvation number in the following form:

$$SN = \frac{Ca}{O_{SR}} \cdot \frac{1}{2\,K \cdot \pi} \cdot \begin{cases} 1 & \text{if } x \leq x_{SW} \\ \frac{\frac{x_c}{x}-1}{\frac{x_c}{x_{SW}}-1} & \text{if } x_c \geq x > x_{SW} \\ 0 & \text{if } x > x_c \end{cases} \tag{10}$$

where $K = \frac{b}{a}$ is the elliptical ratio of the contact. This formulation is subject to the assumption that the entrainment velocity $v_{ent,max}$ takes the role of the velocity v responsible for the viscous shear in the Ca-number. The comparison with the literature shows that capillary effects play a role in the lubrication of contacts by driving the supply of the inlet meniscus [34]. Recent publications employing VOF-methods show also a strong dependency of distinctive meniscus features on the Ca-number [35,36]. Chen et al. explain the dependency on the capillary number by the force balance between capillary and viscous forces at the leading edge of the meniscus based on numerical investigations [35]. Although such effects can play a role in this case under oscillating conditions and probably boundary or mixed friction, this explanation is not strictly compatible with the ideas of Wandel et al. [25]. They used the viscosity in their formulation of the starvation number to express the resistance of base oil against replenishment of the area around the contact. Therefore, the shear of the oil during replenishment is not caused by the entertainment speed, and its use as the shear speed is not entirely in line with Wandel's theory. Nevertheless, such mechanisms

concerning the meniscus around the contact could occur in connection with Wandel et al.'s theory. Several studies have already implemented the non-newtonian flow behaviour of grease into VOF-algorithms to study grease flow in ball bearings or other machine elements and brought interesting insight into the distribution of grease in these systems [37–40]. Nevertheless, the role of the bleeding of the base oil remains unclear in these models. A comprehensive numerical method that models all of the relevant effects, including three-phase flow around the contact, mixed lubrication conditions, and the onset of wear has not been implemented in the literature due to the complicated nature of multiphysics modelling [1].

Thus far, the theory of Wandel et al. [21,25] and the explanations in this paper focus solely on the base oil flow and interpret the thickener as a base oil reservoir next to the track. Cann showed that grease thickener forms a lubricating layer at rolling speeds comparable to the speeds in this investigation [41]. Although the contact pressures in this investigation are higher compared to Cann, it is desirable to analyse the role of this thickener layer for the current application. Furthermore, the starvation number is not yet validated regarding the influence of the surface tension σ_S between the base oil and air. In addition, differences regarding the wettability of the base oil on the raceways and the cage are not incorporated into the starvation number. From the standpoint of established theory, wettability will influence base oil replenishment and therefore also wear initiation [42]. These effects can become relevant when applying the starvation number to hybrid or all-ceramic rolling element bearings. Basically, the general concept is transferable to different bearing materials since the underlying principle of displacement and replenishment is also applicable to changed materials. As mentioned, care needs to be taken regarding the critical value of the starvation number since different wettability can have an influence on the replenishment. Furthermore, the development of the torque ratio in the case of damage can change due to altered wear mechanisms of ceramic components [43].

As all results regarding the starvation number are based on experiments with constant operating conditions; it is questionable how it can be applied in applications with dynamically changing operating conditions, such as wind turbine applications. Hence, the influence of non-constant operating parameters needs to be further investigated. In contrast to the static loading and constant oscillation parameters of the herein-discussed experiments, blade bearings are subjected to varying loads that can lead to a change in contact angle and therefore also a change in the stressed contact area. Furthermore, the effect of alternating oscillation parameters above and below the critical starvation threshold, in addition to the changing loads, are not yet foreseeable.

5. Conclusions

The aim of this paper was to investigate whether the starvation number of WANDEL ET AL., derived from small-scale testing of ACBBs, is also applicable to larger bearing sizes and line contacts. Analysing the conducted experiments on greased, oscillating bearings for line contacts and larger size (pitch diameter of 673 mm) confirms the previous understanding of Wandel et al.: the higher the oscillation frequency, the higher the risk of wear initiation. For the influence of the double amplitude, there are three distinctive regimes: first, an increase in amplitude also increases the wear initiation in the bearing; second, the opposite is the case and finally after a certain double amplitude wear is not encountered anymore. A critical starvation number of $SN_{crit} = 1$ delivered good results for predicting the occurrence of wear throughout all of the four different types and sizes of bearings. A direct comparison between line and point contact reveals that the naturally longer contact length perpendicular to the rolling direction leads to a higher risk of oscillating wear. The extension of the experimentally validated range of bearing sizes and types for the starvation number enables its use as an indication for bearing design. Moreover, the results can also be useful in the context of hybrid bearings, although validation is required. In addition, it should be mentioned that currently there is also no direct way to determine the double amplitude corresponding to x_c reliably in advance,

which makes experiments for the application of the starvation number to a new bearing type necessary. The results of the SBB are especially interesting for large-scale slewing bearings such as blade bearings. It is shown that the starvation number can be used to assess certain parameters of oscillating operation conditions with respect to the risk of wear. Hence, it could be possible to use the starvation number as a design criterion when tuning a pitch controller. However, more work in connection with data from field applications is necessary for validation. Data such as this can provide an answer as to whether there is a correlation between blade bearings suffering from false brinelling and pitch activity, leading to high starvation numbers frequently. In this context, future research in this field should focus on the dynamically changing operation conditions and their order of occurrence. To complement the results of the SBB with further testing on small-scale bearings, future research could also focus on the influence of sealed bearings on grease distribution and the regimes of the starvation number.

Author Contributions: Conceptualisation, G.B., A.B., S.W., S.B. and G.P.; formal analysis, G.B., A.B. and S.W.; funding acquisition, A.B., S.W. and G.P.; investigation, G.B., A.B. and S.W.; methodology, G.B., A.B., S.W. and S.B.; project administration, A.B., S.W., S.B. and G.P.; resources, G.B., A.B., S.W. and G.P.; supervision, S.W. and G.P.; validation, G.B., A.B., S.W. and S.B.; visualisation, G.B., A.B., and S.W.; writing—original draft, G.B. and A.B.; writing—review and editing, G.B., A.B., S.W., S.B. and G.P. All authors have read and agreed to the published version of the manuscript.

Funding: This document is a result of the research projects "iBAC—intelligent Blade Bearing Amplitude Control" (grant number 0324344A), "HAPT2—Beschleunigte Prüfung von Blattlagern für Multi-Megawatt-Turbinen: Rollenlager als Rotorblattlager" (grant number 03EE2033B) funded by the Federal Ministry for Economic Affairs and Climate Action (Federal Republic of Germany) and of the project "Designkonzept für langlebige schwingend beanspruchte oszillierende Wälzlager an Windenergieanlagen" funded by the Bremer Aufbau-Bank GmbH (grant number VE0125A).

Data Availability Statement: The data presented in this study are available on request from the corresponding author.

Acknowledgments: The authors would like to thank Marcel Lohmann and Hazem Ibrahim, as well as Heinrich Drath and Nils Thormälen, for their support in assembling the bearings for the experiments.

Conflicts of Interest: The authors declare no conflict of interest. The funders had no role in the design of the study; in the collection, analyses, or interpretation of data; in the writing of the manuscript; or in the decision to publish the results.

Abbreviations

The following abbreviations are used in this manuscript:

4P BB	Four-Point Ball Bearing
ACBB	Angular Contact Ball Bearing
CRTB	Cylindrical Roller Thrust Bearing
DGBB	Deep Groove Ball Bearing
IPC	Individual Pitch Control
RE	Rolling Element
SBB	Scaled Blade Bearing
SEM	Scanning Electron Microscope
STM	Scanning Tunneling Microscopy
TBB	Thrust Ball Bearing
VOF	Volume of Fluid

Nomenclature

a	Long HERTZ'ian half axis (L)
b	Short HERTZ'ian half axis (L)
Ca	Capillary number
f	Oscillation frequency (T^{-1})
f_c	Critical oscillation frequency (T^{-1})
K	Elliptical ratio
M_y	Load Bending Moment ($M\,L^2\,T^{-2}$)
O_{SR}	Bleeding rate of the grease
R	Rolling element radius (L)
r_p	Pitch radius (L)
SN	Empirical starvation number
T	Friction torque of test bearings ($M\,L^2\,T^{-2}$)
T_{rec}	Measured torque value ($M\,L^2\,T^{-2}$)
T_{acc}	Inertia torque of oscillating parts ($M\,L^2\,T^{-2}$)
$T_{f,sup}$	Friction torque not originating from rolling contacts ($M\,L^2\,T^{-2}$)
v	Fluid speed ($L\,T^{-1}$)
$v_{ent,max}$	Maximum entrainment speed in one period ($L\,T^{-1}$)
x	Travelled distance of rolling element between dead centres (L)
x_{SW}	Travelled distance where secondary lubrication sets in (L)
x_c	Travelled distance where wear is prevented (L)
α	Contact angle
η_0	Dynamic base oil viscosity ($M\,L^{-1}\,T^{-1}$)
λ	Ratio of effective radii
ν	Kinematic base oil viscosity ($L^2\,T^{-1}$)
σ_s	Surface tension between base oil and air ($M\,T^{-2}$)
Φ	Angular position of inner ring
φ	Double amplitude of the inner ring angle
$\omega_{i,max}$	Absolute maximum angular velocity of inner ring during one period (T^{-1})
$\omega^*_{i,max}$	Relative maximum angular velocity of inner ring during one period (T^{-1})

Appendix A

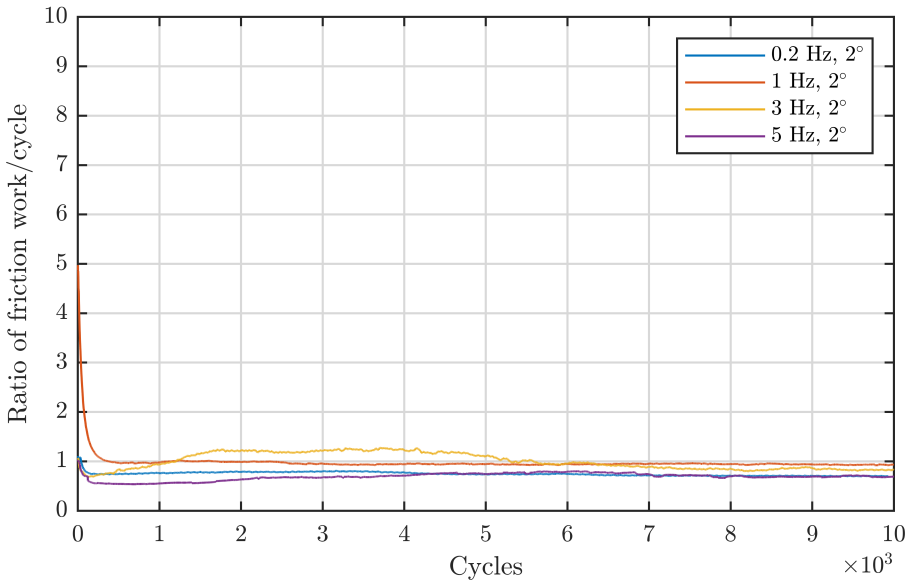

Figure A1. Frequency influence for type 7312 bearings at a double amplitude of 2°.

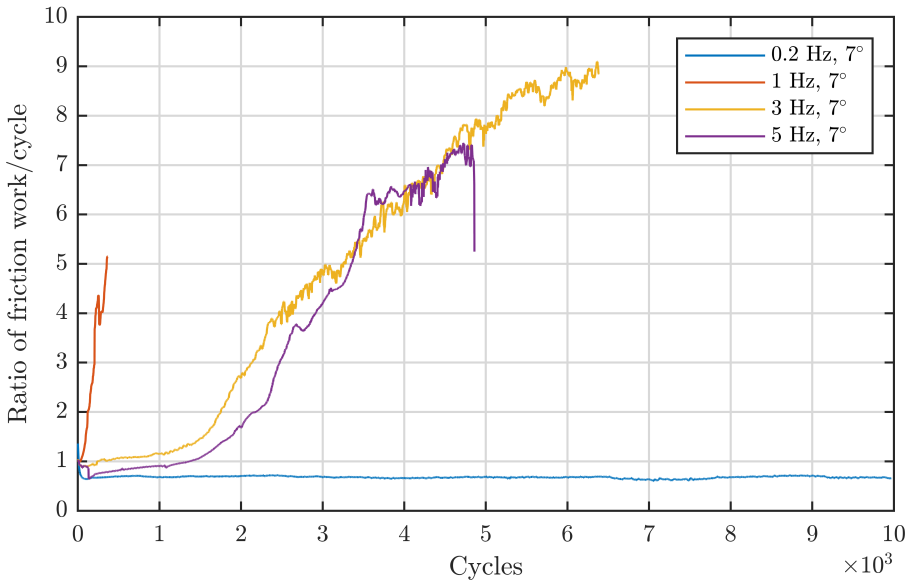

Figure A2. Frequency influence for type 7312 bearings at a double amplitude of 7°.

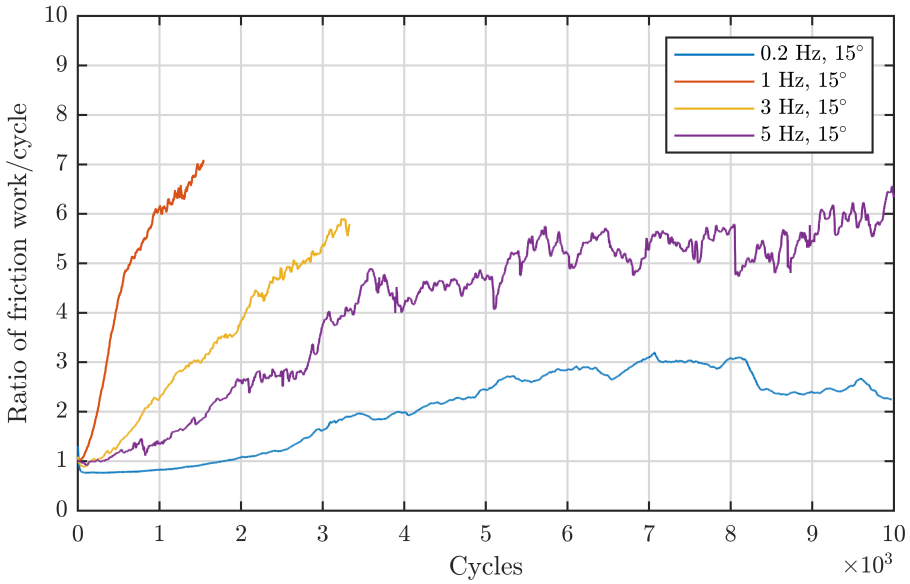

Figure A3. Frequency influence for type 7312 bearings at a double amplitude of 15°.

Table A1. Additional test parameters for type 81212 bearings.

Double Amplitude φ in °	**Frequency f in Hz**
1.139	0.2
1.139	5
6	0.2
6	0.7
6	0.5
6	0.3
6	0.4

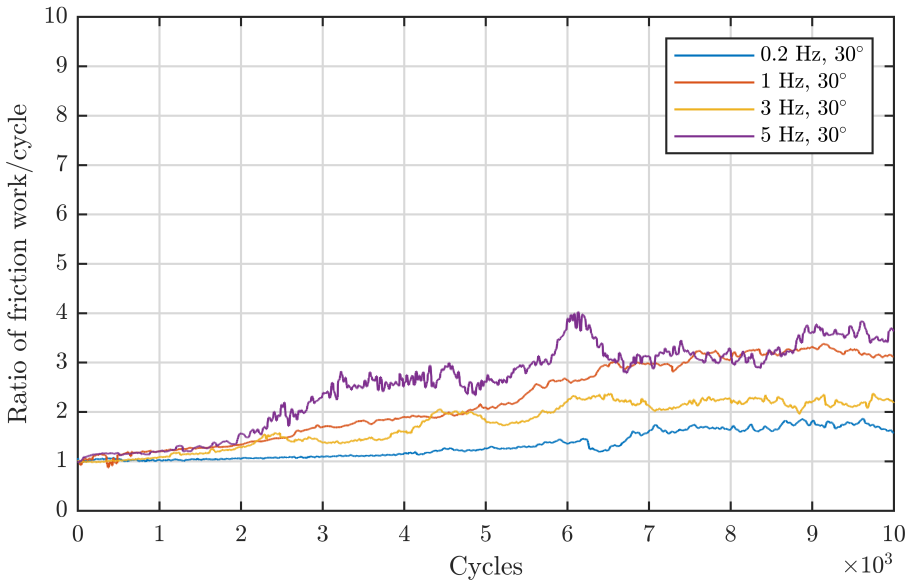

Figure A4. Frequency influence for type 7312 bearings at a double amplitude of 30°.

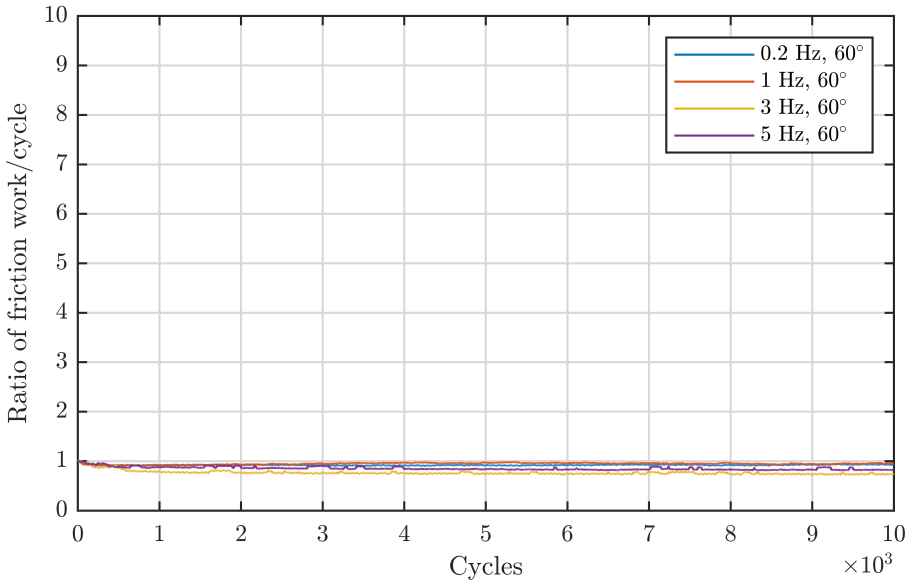

Figure A5. Frequency influence for type 7312 bearings at a double amplitude of 60°.

Table A2. Regime thresholds for Figures 16 and 17.

Bearing Type	φ Corresponding to x_{sw}	φ Corresponding to x_c
81212	11°	35°
SBB	2.25°	7.5°
7312	7°	60°
7208	15°	30°

References

1. Lugt, P.M. A review on grease lubrication in rolling bearings. *Tribol. Trans.* **2009**, *52*, 470–480. [CrossRef]
2. Han, J.W.; Nam, J.S.; Park, Y.J.; Lee, G.H.; Nam, Y.Y. An experimental study on the performance and fatigue life of pitch bearing for wind turbine. *J. Mech. Sci. Technol.* **2015**, *29*, 1963–1971. [CrossRef]
3. Cubillas, D.; Olave, M.; Llavori, I.; Ulacia, I.; Larrañaga, J.; Zurutuza, A.; Lopez, A. Numerical analysis of the wind turbine pitch bearing raceway tribo-contact due to cyclic loading under constant pitch angle. In Proceedings of the Fracture, Fatigue and Wear, Singapore, 2–3 August 2021; pp. 757–769.

4. Lopez, A.; Zurutuza, A.; Olave, M.; Portugal, I.; Muñiz-Calvente, M.; Fernandez-Canteli, A. Pitch bearing lifetime prediction considering the effect of pitch control strategy. *Proc. J. Phys. Conf. Ser.* **2019**, *1222*, 012017. [CrossRef]
5. Liu, Z.; Wang, X.; Zhang, L. Fault diagnosis of industrial wind turbine blade bearing using acoustic emission analysis. *IEEE Trans. Instrum. Meas.* **2020**, *69*, 6630–6639. [CrossRef]
6. Morisse, M.; Bartschat, A.; Wenske, J.; Mertens, A. Impact of individual pitch control on pitch actuators in megawatt wind turbines. In Proceedings of the 2017 19th European Conference on Power Electronics and Applications (EPE'17 ECCE Europe), Warsaw, Poland, 11–14 September 2017; pp. 1–9.
7. Grebe, M.; Molter, J.; Schwack, F.; Poll, G. Damage mechanisms in pivoting rolling bearings and their differentiation and simulation. *Bear. World J.* **2018**, *3*, 71–86.
8. Schadow, C. *False Brinelling—Stillstehende fettgeschmierte Wälzlager unter dynamischer Belastung*; Abschlussbericht FVA-Nr. 540 I, Otto-von-Guericke-Universität Magdeburg Institut für Maschinenkonstruktion (IMK); FVA: Frankfurt, Germany, 2010.
9. Schadow, C. *False Brinelling—Stillstehende fettgeschmierte Wälzlager unter dynamischer Belastung*; Abschlussbericht FVA-Nr. 540 II, Otto-von-Guericke-Universität Magdeburg Institut für Maschinenkonstruktion (IMK); FVA: Frankfurt, Germany, 2015.
10. Tetora, S. *False Brinelling—Stillstehende fettgeschmierte Wälzlager unter dynamischer Belastung*; Abschlussbericht FVA-Nr. 540 III, Otto-von-Guericke-Universität Magdeburg Institut für Maschinenkonstruktion (IMK); FVA: Frankfurt, Germany, 2022.
11. Schwack, F.; Bader, N.; Leckner, J.; Demaille, C.; Poll, G. A study of grease lubricants under wind turbine pitch bearing conditions. *Wear* **2020**, *454*, 203335. [CrossRef]
12. Phaner-Goutorbe, M.; Barthou, C.; Porte, L.; Vannes, B. Scanning tunneling microscopy study of wear induced by false brinelling on rolling bearings. *Appl. Surf. Sci.* **1997**, *108*, 45–51. [CrossRef]
13. Maruyama, T.; Saitoh, T.; Yokouchi, A. Differences in mechanisms for fretting wear reduction between oil and grease lubrication. *Tribol. Trans.* **2017**, *60*, 497–505. [CrossRef]
14. Becker, D. *Hoch Belastete Großwälzlagerungen in Windenergieanlagen*; Shaker: Aachen, Germany, 2012.
15. Cavacece, F.; Frache, L.; Tonazzi, D.; Bouscharain, N.; Philippon, D.; Le Jeune, G.; Maheo, Y.; Massi, F. Roller bearing under high loaded oscillations: Life evolution and accommodation mechanisms. *Tribol. Int.* **2020**, *147*, 106278. [CrossRef]
16. Komba, E.H.; Massi, F.; Bouscharain, N.; Le Jeune, G.; Berthier, Y.; Maheo, Y. Experimental damage analysis in high loaded oscillating bearings. *Tribol. Int.* **2016**, *102*, 507–515. [CrossRef]
17. Kato, M.; Sato, T. The development of low friction and anti-fretting corrosion greases for CVJ and wheel bearing applications. *SAE Trans.* **1987**, 1244–1250.
18. Duque, R.G.; Wang, Z.; Duell, D.; Fowler, D.E. ToF-SIMS analysis of anti-fretting films generated on the surface of ball bearings containing dithiocarbamate and dithiophosphate grease additives. *Appl. Surf. Sci.* **2004**, *231*, 342–347. [CrossRef]
19. Pape, F.; Poll, G. Investigations on graphene platelets as dry lubricant and as grease additive for sliding contacts and rolling bearing application. *Lubricants* **2019**, *8*, 3. [CrossRef]
20. Frache, L.; Komba, E.H.; Philippon, D.; Galipaud, J.; De Barros, M.; Douillard, T.; Masenelli-Varlot, K.; Bouscharain, N.; Maheo, Y.; Sarlin, R.; et al. Observation of a modified superficial layer on heavily loaded contacts under grease lubrication. *Tribol. Int.* **2021**, *158*, 106921. [CrossRef]
21. Wandel, S.; Bader, N.; Schwack, F.; Glodowski, J.; Lehnhardt, B.; Poll, G. Starvation and relubrication mechanisms in grease lubricated oscillating bearings. *Tribol. Int.* **2022**, *165*, 107276. [CrossRef]
22. *DIN 623-1*; Wälzlager-Grundlagen—Teil 1: Bezeichnung, Kennzeichnung. Deutsches Institut für Normung e. V.: Berlin, Germany, 2020.
23. *DIN 616*; Wälzlager -Maßpläne. Deutsches Institut für Normung e. V.: Berlin, Germany, 2022.
24. Poll, G.; Li, X.; Bader, N.; Guo, F. Starved lubrication in rolling contacts-a review. *Bear. World J.* **2019**, *4*, 69–81.
25. Wandel, S.; Bader, N.; Leckner, J.; Lehnhardt, B.; Glodowski, J.; Poll, G. Starvation and Relubrication in Oscillating Bearings-Influence of Grease Parameters. *Tribol. Lett.* **2022**, *70*, 114 [CrossRef]
26. *DIN 51817*; Prüfung von Schmierstoffen—Bestimmung der Ölabscheidung aus Schmierfetten unter Statischen Bedingungen. Deutsches Institut für Normung e. V.: Berlin, Germany, 2014.
27. *DIN 51819*; Prüfung von Schmierstoffen—Mechanisch-Dynamische Prüfung auf dem Wälzlagerschmierstoff-Prüfgerät FE8. Deutsches Institut für Normung e. V.: Berlin, Germany, 2016.
28. Menck, O.; Behnke, K.; Stammler, M.; Bartschat, A.; Schleich, F.; Graßmann, M. Measurements and modeling of friction torque of wind turbine blade bearings. *J. Phys. Conf. Ser.* **2022**, *2265*, 022087. [CrossRef]
29. Jacod, B.; Pubilier, F.; Cann, P.; Lubrecht, A. An analysis of track replenishment mechanisms in the starved regime. In *Tribology Series*; Elsevier: Amsterdam, The Netherlands, 1999; Volume 36, pp. 483–492.
30. Damiens, B.; Lubrecht, A.; Cann, P. Influence of cage clearance on bearing lubrication©. *Tribol. Trans.* **2004**, *47*, 2–6. [CrossRef]
31. Harris, T.; Kotzalas, M. *Rolling Bearing Analysis: Essential Concepts of Bearing Technology*; CRC Press: Boca Raton, FL, USA, 2004.
32. Wandel, S.; Bartschat, A.; Glodowski, J.; Bader, N.; Poll, G. Wear Development in Oscillating Rolling Element Bearings. *Lubricants* **2023**, *11*, 117. [CrossRef]
33. Guo, H.; Song, K.; Hilfer, R. A Brief Review of Capillary Number and its Use in Capillary Desaturation Curves. *Transp. Porous Media* **2022**, *144*, 3–31. [CrossRef]
34. Li, X.; Guo, F.; Wong, P.; Zhao, Y. Regulation of lubricant supply by wettability gradient in rolling EHL contacts. *Tribol. Int.* **2018**, *120*, 565–574. [CrossRef]

35. Chen, H.; Wang, W.; Liang, H.; Zhao, Z. Patterns of interfacial flow around a lubricated rolling point contact region. *Phys. Fluids* **2021**, *33*, 102118. [CrossRef]
36. Fischer, D.; von Goeldel, S.; Jacobs, G.; Stratmann, A. Numerical investigation of effects on replenishment in rolling point contacts using CFD simulations. *Tribol. Int.* **2021**, *157*, 106858. [CrossRef]
37. Mastrone, M.N.; Concli, F. CFD simulation of grease lubrication: Analysis of the power losses and lubricant flows inside a back-to-back test rig gearbox. *J. Non-Newton. Fluid Mech.* **2021**, *297*, 104652. [CrossRef]
38. Blanco, A.M.; Oro, J.F. Unsteady numerical simulation of an air-operated piston pump for lubricating greases using dynamic meshes. *Comput. Fluids* **2012**, *57*, 138–150. [CrossRef]
39. Noda, T.; Shibasaki, K.; Miyata, S.; Taniguchi, M. X-ray CT imaging of grease behavior in ball bearing and numerical validation of multi-phase flows simulation. *Tribol. Online* **2020**, *15*, 36–44. [CrossRef]
40. Raj, A.; Sarkar, C.; Pathak, M. Thermal and multiphase flow simulations of polytetrafluoroethylene-based grease flow in restricted geometry. *Proc. Inst. Mech. Eng. Part J J. Eng. Tribol.* **2022**, *236*, 80–89. [CrossRef]
41. Cann, P. Grease lubrication of rolling element bearings—role of the grease thickener. *Lubr. Sci.* **2007**, *19*, 183–196. [CrossRef]
42. Ge, D.; Deng, J.; Duan, R.; Li, X.; Liu, Y.; Yue, H. Effect of surface wettability on tribological properties of Al_2O_3/TiC ceramic under wet lubrication. *Ceram. Int.* **2019**, *45*, 24554–24563. [CrossRef]
43. Lugt, P.M.; van Zoelen, M.T.; Vieillard, C.; Berens, F.; Gruell, R.; Preisinger, G.; Meaney, P. Grease performance in ball and roller bearings for all-steel and hybrid bearings. *Tribol. Trans.* **2021**, *65*, 1–13. [CrossRef]